



HAL
open science

Custom 3D Printed Spatial Atomic Layer Deposition Manifold for the Coating of Tubular Membranes

Fidel Toldra-Reig, Clément Lausecker, Matthieu Weber, Mikhael Bechelany,
David Muñoz-Rojas

► **To cite this version:**

Fidel Toldra-Reig, Clément Lausecker, Matthieu Weber, Mikhael Bechelany, David Muñoz-Rojas. Custom 3D Printed Spatial Atomic Layer Deposition Manifold for the Coating of Tubular Membranes. *ACS Sustainable Chemistry & Engineering*, 2022, 10 (43), pp.14112-14118. 10.1021/acssuschemeng.2c04424 . hal-03852184

HAL Id: hal-03852184

<https://hal.umontpellier.fr/hal-03852184v1>

Submitted on 14 Nov 2022

HAL is a multi-disciplinary open access archive for the deposit and dissemination of scientific research documents, whether they are published or not. The documents may come from teaching and research institutions in France or abroad, or from public or private research centers.

L'archive ouverte pluridisciplinaire **HAL**, est destinée au dépôt et à la diffusion de documents scientifiques de niveau recherche, publiés ou non, émanant des établissements d'enseignement et de recherche français ou étrangers, des laboratoires publics ou privés.

Custom 3D Printed Spatial Atomic Layer Deposition Manifold for the Coating of Tubular Membranes

Fidel Toldra-Reig^{a,†,}, Clément Lausecker^{a,b}, Matthieu Weber^a, Mikhael Bechelany^b and David
Muñoz-Rojas^{a,**}*

^a Univ. Grenoble Alpes, CNRS, Grenoble INP, LMGP, F-38000 Grenoble, France

^b Institut Européen des Membranes, IEM, UMR-5635, Univ. Montpellier, CNRS, ENSCM, Place
Eugène Bataillon 34095 Montpellier cedex 5, France

Abstract

The development of highly efficient membranes represents a great opportunity to significantly reduce the environmental impacts of human activities through gas separation and water filtration, and are also very attractive for process intensification when coupled to existing industrial processes. Tubular membranes have higher modularity, better pressure resistance, and they offer easier sealing than their flat counterparts. The ability to deposit thin films on their surface is crucial to optimize their chemical and physical properties. However, the deposition of thin films on tubular membrane supports with conventional vacuum-based deposition techniques is relatively complex, slow and costly. In this work the versatility of spatial atomic layer deposition (SALD) and 3D printing technologies has been combined to design and fabricate a custom SALD manifold for coating tubular substrates. SALD is a scalable deposition technique, offering high-throughput at atmospheric pressure and thus can be advantageously employed to coat tubular membranes, enabling high quality thin films to be deposited at the nanoscale considerably faster than with other conventional techniques. Computational fluid dynamics (CFD) calculations by means of COMSOL Multiphysics have been used to optimize this innovative SALD gas manifold. The proof-of-concept of the new SALD manifold has been validated through successful ZnO thin film depositions performed on tubular Cu foils and porous Al₂O₃ tubular membrane supports, demonstrating the capability of SALD to achieve high-throughput depositions on non-planar, complex

25 substrates. These results open prospects for the interface engineering of membranes or electrolyzers,
26 where precise coatings of tubular surfaces are needed.

27 **Keywords**

28 Inorganic membrane, Spatial Atomic Layer Deposition, 3D printing, tubular substrates, interface
29 engineering

30

31 **1. Introduction**

32 The development of highly efficient membranes has become of central interest for the energy sector
33 and the chemical industry, as the efficient separation of species represents a valuable strategy to reduce
34 cost, energy, and environmental impact of many processes^{1,2} or to reduce the impact of human activities
35 by elimination of pollutants in wastewater and contaminated air. One example of current membrane energy
36 application is the membrane-assisted separation of hydrogen for its use as energy carrier³⁻⁸, which is
37 expected to be fundamental for the forthcoming shift to carbon-neutral societies. Coupling membranes to
38 chemical industry is a key strategy for intensification of processes such as Fischer-Tropsch, aromatization,
39 de/hydrogenation, reforming⁹⁻¹² and membrane reactors in general¹³.

40 The separation processes are achieved by enabling species/molecules to pass through the membrane
41 as a result of a driving force. Most transport processes take place because of a difference in chemical
42 potential (pressure and concentration contribute to the chemical potential). Depending on their
43 architecture, membranes achieve fluid separation through either i) solution-diffusion, if a dense film of
44 the appropriate material is used, or ii) molecular sieving, for appropriate porous films. In particular,
45 tubular-shaped membranes are appealing to industry since they offer strong adaptability, easier sealing,
46 high-pressure resistance and higher modularity than their planar counterparts. Such membranes can be
47 prepared by dip-coating or spray-coating of tubular supports by sol-gel routes (plus spin coating or screen
48 printing for planar membranes), but the precise control of chemical and physical properties of both dense
49 and porous membranes (i.e., thickness, surface composition, pore size, etc.) is still a key challenge for
50 membrane producers^{1,2}. Thus, thin films are highly attractive for the coating of dense membranes, as it

51 decreases the amount of material required (especially for expensive or scarce elements) while improving
52 the permeability. In addition, thin film techniques can enable a precise control of the pore size for porous
53 membranes.

54 Among thin film deposition techniques enabling tubular coatings, physical vapor deposition (PVD)
55 techniques have a low energy-efficiency and spinning systems are required (including heating elements)
56 which increase the complexity and/or cost. Electrodeposition and solvothermal approaches can be used
57 for the deposition of metals and simpler oxides with lower use of consumables and at lower cost. However,
58 these approaches require more steps, yield thicker layers and there are also several concerns from the
59 health, safety and environmental points of view ¹>. As recently reviewed, chemical vapor deposition
60 (CVD) techniques such as atomic layer deposition (ALD) are extremely valuable for membrane science
61 and have been tested for many applications, including gas separation and water filtration, biosensing and
62 catalysis ¹⁵⁻¹⁷. ALD is based on the sequential use of surface-limited, self-terminating chemical reactions
63 that take place in a cycle-wise fashion, thus allowing to prepare conformal and high quality films at the
64 nanoscale on complex substrates and at low temperatures ¹⁸⁻²⁰. ALD has traditionally been a vacuum-
65 based technique requiring the use of relatively costly reactors and pumping systems. Spatial atomic layer
66 deposition (SALD) is a branch of conventional ALD, in which the precursors are continuously injected
67 in different locations of the reactor, being separated by a flow of inert gas. This technique is able to reach
68 faster growth rates than conventional ALD and can be performed at atmospheric pressure and in the open
69 air (i.e. without deposition chamber) ^{21,22}. This does not compromise the deposition of high quality
70 materials, even on high-aspect -ratio substrates, with precise thickness control, high uniformity and
71 excellent conformality ²³⁻²⁵.

72 SALD can indeed be implemented in different ways ²>. This work is based on the close-proximity
73 manifold approach ^{27,28}, where the reactants are distributed along adjacent channels and separated by inert
74 gas and exhausts channels ²⁹. The close proximity of the substrate to the head then ensures the efficient
75 separation of the reactants. The movement of the substrate exposes the surface to the different reactants,
76 therefore reproducing the layer-by-layer growth of conventional ALD. This SALD approach is

77 particularly versatile since it can be easily tuned by simply modifying the manifold injector. For instance,
78 we have shown that 3D printing can be used to customize close-proximity SALD manifolds in different
79 materials, opening up a large span of possibilities ^{30,31}.

80 However, SALD has been only used to coat planar substrates such as wafers, glasses, or flat
81 polymeric substrates so far. Porous materials or high-aspect-ratio features have also been coated, but the
82 macroscopic nature of these samples is a flat substrate. A notable exception has been reported van
83 Ommen's group where the coating of nanoparticles was enabled by implementing a SALD system in a
84 fluidized reactor ³². In this work, we take advantage of 3D printing to design a gas manifold specifically
85 tailored for tubular supports. To demonstrate the feasibility to perform SALD on such tubular surfaces,
86 ZnO layers have been deposited on Cu foils wrapped around tubular supports and on Al₂O₃ tubular porous
87 membrane substrates. This work is a new versatile way of printing functional devices to extend the current
88 potential of SALD³³⁻³⁵ to membrane applications, opening a new avenue in the field for coating complex
89 substrates with functional materials.

90 **2. Materials and Methods**

91 *2.1. SALD of ZnO on tubular supports*

92 The gas manifold was elaborated through computer-aided design (CAD) in Solid Edge and 3D printed
93 by stereolithography (FORM2, Formlabs) with Clear V4 (Formlabs). Supports and resin leftovers were
94 carefully removed and the 3D-piece was cleaned with isopropanol (<99.8% purity, Honeywell) and
95 cautiously dried prior to SALD deposition. Simulations of the gas pressure distribution among the
96 prechambers and gas outlet channels within the SALD gas manifolds were performed in COMSOL
97 Multiphysics software using the CFD module.

98 ZnO was deposited at room temperature using a custom-made atmospheric pressure SALD system
99 ^{3>}. Two substrates were considered : i) Cu foils (3M) wrapped around 3D printed polymer tubes of 1 cm
100 diameter, and ii) commercial Al₂O₃ porous tubular membranes (50 nm pore size diameter, Atech
101 Innovations GmbH) of 1 cm outer diameter. Diethylzinc (DEZ, Zn(C₂H₅)₂, Sigma Aldrich) and water

102 (H₂O) were used as metal precursor and coreactant respectively. Nitrogen (99.995%, AirLiquide) was
103 used both as a carrying gas in precursor lines and as barrier gas in dedicated lines separating DEZ and
104 water flows. The precursors were carried from the bubblers to the gas manifold by flowing 15 and 90
105 sccm of nitrogen through the DEZ and water bubblers, and were subsequently diluted with 135 and 210
106 sccm of additional nitrogen, respectively. The total nitrogen flowrate used as barrier gas was 600 sccm.

107 *2.2. Characterization Techniques*

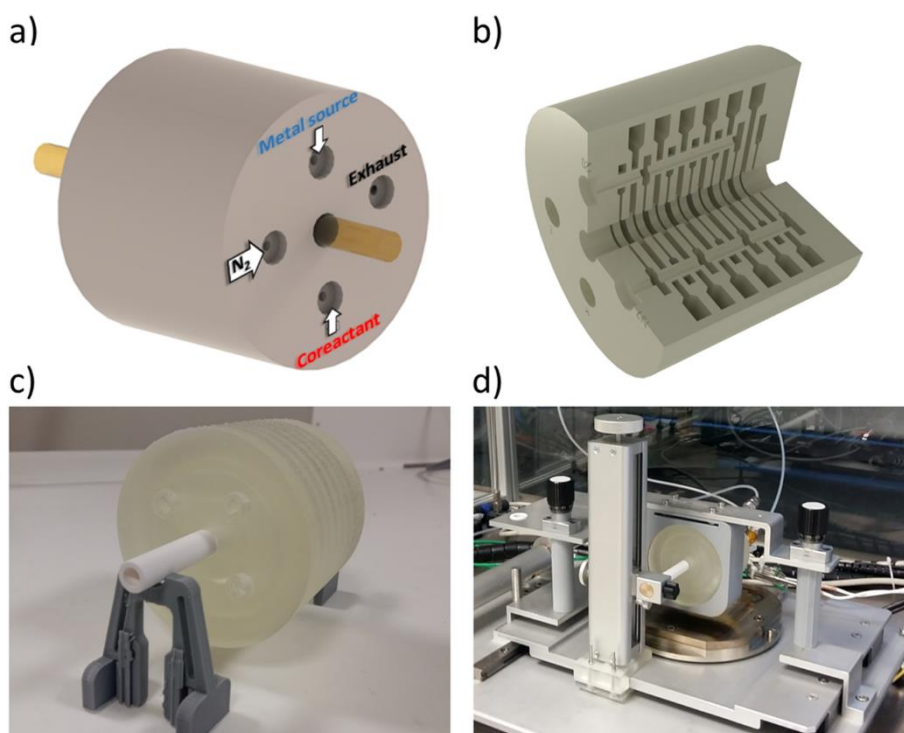
108 The morphology of the deposited ZnO thin films was investigated by field-emission scanning electron
109 microscopy (FESEM) using a Zeiss Gemini 300 field-emission-gun scanning electron microscope.
110 FESEM energy-dispersive X-ray spectroscopy (EDS) spectra were recorded using a Bruker X-ray
111 detector incorporated in the Zeiss Gemini 300 field-emission-gun scanning electron microscope operating
112 at 15 kV. X-ray diffraction (XRD) patterns were collected with a Rigaku SmartLab diffractometer
113 equipped with a rotating Cu anode operating at 9 kW (45 kV and 200 mA) from which the Cu K α ₁
114 radiation was used. The θ -2 θ scans were performed in the standard Bragg–Brentano configuration with a
115 step of 0.1° and a speed of 0.3° s⁻¹ using parallel beams (divergence less than 0.05°). The ZnO and α -
116 Al₂O₃ diffraction peaks were indexed according to the ICDD 00-036-145 and 00-046-1212 files,
117 respectively.

118 **3. Results and Discussion**

119 *3.1. Design and fabrication of the tubular gas manifold*

120 The possibility to 3D print gas manifolds enable the integration of gas distribution and separation
121 circuits into the body as shown in our group previously^{30,31}. In this work, we take further advantage of
122 these capabilities to design a gas manifold for deposition on tubular substrates based in the same close-
123 proximity technology. More specifically, a cylindric gas manifold dedicated to the SALD of tubular
124 surfaces was fabricated through CAD and 3D printing, as illustrated in Fig. 1. The gas manifold contains
125 four external connections, as revealed by Fig. 1a, being the inlets for metal precursor, coreactant, inert
126 gas, and the exhaust outlet. In this configuration, the tubular substrate is introduced in the central

127 cylindrical hole of the gas manifold and moves back and forth during deposition to ensure the exposition
128 of its surface to the different gases. The hole diameter can be easily adjusted to the substrate diameter in
129 order to have a controlled gap in the range of 50-200 μm between the substrate surface and the gas outlets.
130 Furthermore, both inlet and outlet channels connect to individual concentric prechambers located within
131 the the bulk of the gas manifold as detailed in the cross-section view shown in Fig. 1b. These prechambers
132 have a concentric outlet channel facing the substrate to ensure the exposure of the substrate to the gases
133 or to extract them.

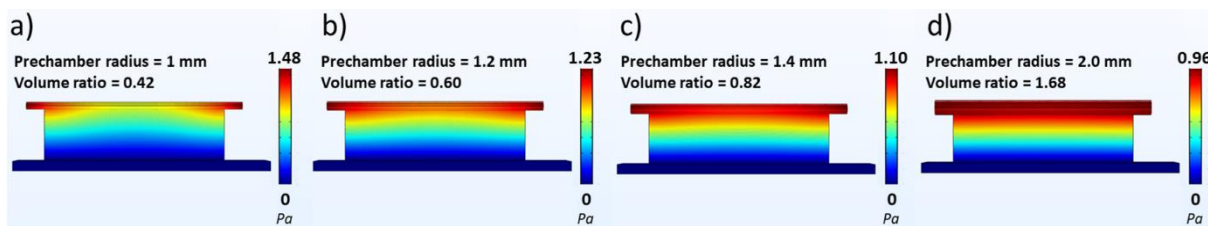


134

135 **Fig. 1.** (a) Scheme of the cylindrical SALD manifold designed to coat tubular substrates, (b) detailed
136 cross-section view of the design, (c) printed version of the gas manifold, and (d) integration into the
137 custom-made SALD system.

138 The concentric prechambers are required to ensure a good homogeneization of the gas pressure and
139 its proper distribution through the outlet channel. An inappropriate design would lead to inhomogeneous
140 deposition with unexposed areas on the tubular substrate ³⁵. Prior to the design, COMSOL Multiphysics
141 simulations using the CFD module were performed to find adequate ratios between the prechamber and
142 the channel outlet volumes offering optimal gas pressure distributions, whose results are summarized in
143 Fig. 2. The study was performed on an individual 3D channel of a standard SALD gas manifold ³⁹ for the

144 sake of time and hardware requirements. There are two inlets in each side of the prechamber, and one
 145 outlet at the bottom of the channel where the substrate is located. As stated before, the flow and pressure
 146 through the prechamber and channel outlet are evaluated to check the size of prechamber yielding a good
 147 homogeneity of the gas, i.e. a constant flow front reaching the substrate surface. **Otherwise, preferential**
 148 **pathways, extended regions with different gas speeds, or dead zones where no gas flow occur can be**
 149 **generated, leading to an innacurate gas distribution and a lack of homogeneity in the deposition.** To do
 150 so, the channel outlet volume was kept constant (with channel dimensions fixed at $50 \times 15 \times 0.5 \text{ mm}^3$)
 151 and the radius of the prechamber was varied from 1 to 2 mm. Moreover, a constant flowrate of 100 mL/min
 152 was applied to both prechamber inlets. The results reveal that a small prechamber volume (i.e. with a
 153 radius of 1 mm, Fig. 2a) should be avoided as it produces very inhomogeneous gas flow distribution along
 154 the outlet channel. The homogeneity of the gas is drastically improved when increasing the prechamber
 155 volume (i.e. when increasing its radius above 1 mm, Fig. 2b-d), a minimum radii between 1.4 and 2 mm
 156 is required to ensure good homogeneization (Fig. 2c,d). Therefore, as a general rule, a prechamber/channel
 157 outlet volume ratio of at least 0.8 should be respected for the design of the cylindrical SALD manifold.



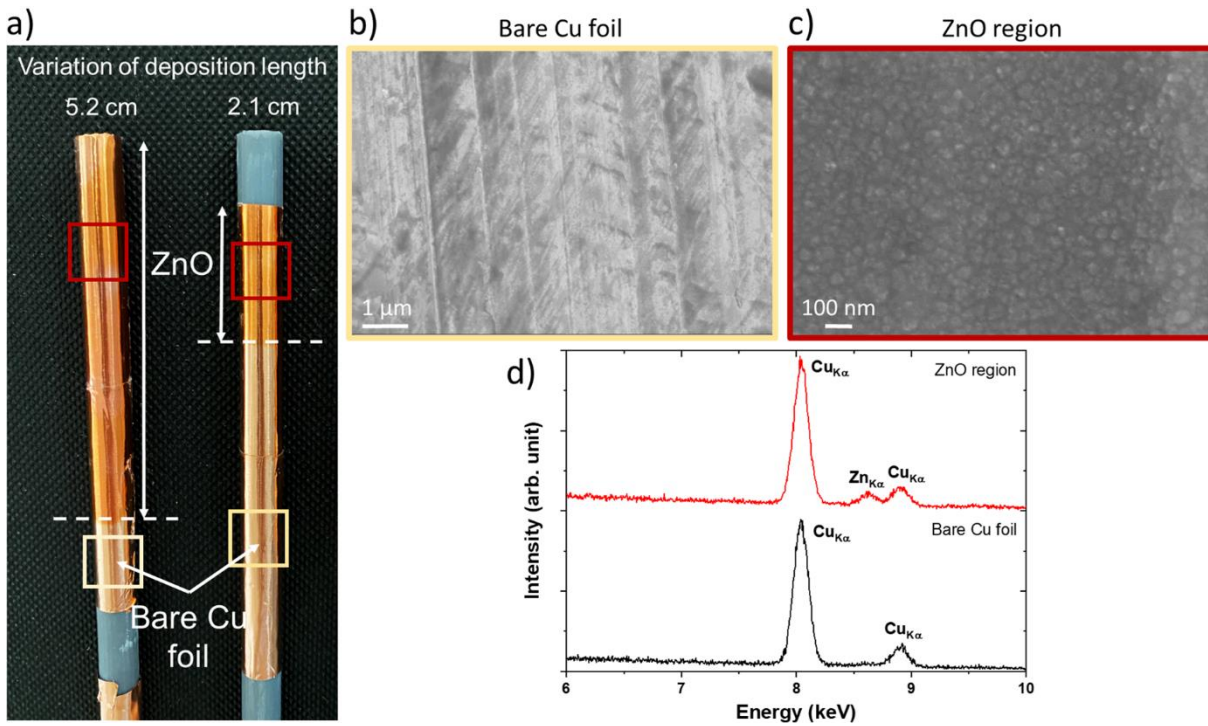
158
 159 **Fig. 2.** CFD calculations made with COMSOL Multiphysics, where the fluid distribution is assessed along
 160 an outlet channel for varying prechamber radii of (a) 1 mm, (b) 1.2 mm, (c) 1.4 mm, and (d) 2.0 mm. The
 161 corresponding prechamber/channel outlet volume ratios are also indicated.

162 The concentric nature of the gas manifold also adds some complexity to the 3D printing process.
 163 Indeed, to guarantee its feasibility, temporary supports must be printed in the central hole where the
 164 substrate is to be placed. However, the smoothness of this internal surface is capital for the deposition
 165 process ensuring an even distribution of the flow. The supports were thus removed carefully and the
 166 internal cylindrical surface was polished with fine polishing paper (1200) to smooth the surface.
 167 Additionnally, a thorough cleaning of the inner channels with isopropanol followed by a drying process

168 must be done to avoid any loss of shape or blockage of the outer channels due to resin or liquid
169 accumulation. A Dino-Lite RK-10 holder with integrated z-axis controller is used as a sample holder to
170 accurately control the height of the tubular sample, providing precise alignment with the gas manifold.
171 The sample holder is secured by a 3D printed home-made piece to the SALD moving plate, tightening the
172 tubular sample at its position at the center of the gas manifold and ensuring an appropriate gap with gas
173 outlets (Fig. 1d).

174 3.2. SALD of ZnO on tubular substrates

175 A first validation of the gas manifold design and integration into the SALD system was performed
176 using 3D printed tubes of 1 cm diameter wrapped with Cu foils as tubular substrates. Cu foils permit the
177 visual identification of the deposition through their change of contrast, and they can be easily unwrapped
178 from the 3D printed tubes for later characterization in SEM. ZnO was chosen because it is a school-case
179 ALD material and because the group has extensive expertise in its deposition ^{36,39}. Additionally,
180 amorphous ZnO can be grown at room temperature facilitating the operational validation of the gas
181 manifold. Standard SALD conditions previously reported for ZnO deposition (^{36,39} on planar substrates)
182 were tested successfully as depicted in Fig. 3a. The deposition distance (i.e. the amplitude of the substrate
183 displacement) was varied and the related changes of contrast observed confirm that the deposition is
184 taking place in the desired region, which can thus be typically controlled in the range of a few centimeters.
185 Moreover, FESEM observations of the Cu foils (Fig. 3b,c) confirm the growth of a ZnO thin film in the
186 region exposed to precursors, while no ZnO is observed in the pristine region. The ZnO layer covers the
187 whole surface exposed, with no apparent change between regions. The deposition of ZnO is further
188 confirmed by FESEM-EDS analyses (Fig. 3d), where a significant signal associated to the $Zn_{K\alpha}$ energy
189 transition is observed at around 8.6 keV in the region exposed to precursors, while this signal is absent on
190 the pristine Cu foil.

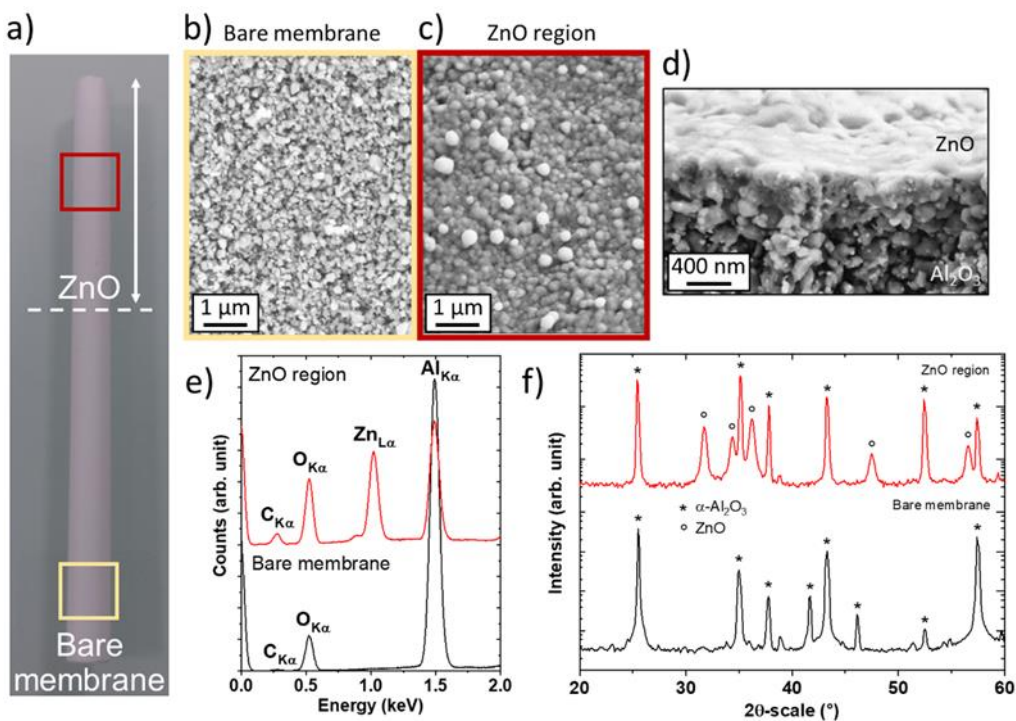


191

192 **Fig. 3.** (a) Cu foils with ZnO depositions along variable lengths. Top-view FESEM images of (b) a bare
 193 Cu foil and of (c) a Cu foil with ZnO deposition. (d) Corresponding FESEM-EDS spectra.

194 In a second step, we aimed to confirm the potential of this new approach for the surface engineering
 195 of membrane supports by using the 3D printed gas manifold to perform SALD on porous α -Al₂O₃ tubular
 196 ceramic supports (50 nm pore size), such as the one presented in Fig. 4a. The equivalent to 1000
 197 conventional ALD cycles were used for deposition of ZnO. FESEM observations revealed the deposition
 198 of a ZnO thin layer with an estimated thickness of 400 nm, corresponding to a growth rate of 4 Å/cycle
 199 (Fig. 4b,c). It can be noted that the growth rate is higher than what is typically expected for an ALD
 200 process, implying a major CVD contribution during the ZnO deposition. Indeed, the possibility to grow
 201 both in CVD and ALD mode is one of the advantages offered by close-proximity SALD based on
 202 manifold heads. Deposition in SCVD mode has been used in the past and, for surfaces with no complex
 203 or high-aspect-ratio features, homogenous films can be obtained with GPC values larger than for the
 204 equivalent ALD process. The optimization of the tubular head presented here is possible for the cases
 205 when ALD conditions are required. These optimizations will involve the adjustment of parameters such
 206 as the flow rates, the gap between the gas manifold and the sample surface, the channel width and
 207 separation, and the sample movement speed. A strong associated signal of the Zn_{Lα} energy transition at

208 around 1.0 eV is further measured from FESEM-EDS characterizations in areas exposed to the chemical
 209 precursors (otherwise absent on the bare membrane), confirming the ZnO chemical nature of the thin layer
 210 (Fig. 4d). Moreover, different membrane pieces were characterized by XRD to gain more insights on their
 211 structural properties. To ensure good crystallization of the ZnO thin film, the samples were annealed at
 212 500 °C during 1 h. The obtained XRD patterns in the deposited region, shown in Fig. 4e, clearly reveal
 213 the presence of several diffraction peaks associated to wurtzite ZnO, while only diffraction peaks
 214 associated to α -Al₂O₃ are present on the bare membrane. These results demonstrate the great potential of
 215 SALD for the deposition of high quality thin films on complex substrates such as tubular membrane
 216 supports. Additionally, the repeatability of the depositions and reuse of the gas manifold can be typically
 217 achieved through a proper alignment of the sample using the level adjuster described previously and a
 218 thorough gas manifold maintenance (cleaning with 5% nitric acid solution, rinsing with isopropanol and
 219 drying), respectively.



220
 221 **Fig. 4.** (a) Tubular membrane support after ZnO deposition. (b,c) Top-view FESEM images of the
 222 membrane (b) without and (c) with ZnO deposition. (d) High-magnification cross-section view of the
 223 ZnO thin film. (e) Corresponding FESEM-EDS spectra, and (f) XRD patterns of membrane pieces without
 224 and with ZnO deposition after annealing at 500 °C.

225 3.3 Perspectives

226 The present work shows a proof of concept reporting the coating of tubular membranes by an an
227 open-air technique (SALD) which is attractive for interface engineering because of both conformal coating
228 and excellent thickness control. For example, some ALD-prepared materials such as palladium or metal-
229 organic frameworks (MOFs) are particularly relevant for the fabrication of separation membranes ^{40,41}. It
230 is worth noting that thin films such as ZnO can be subsequently converted to a MOF by hydrothermal
231 techniques. Heating elements can also be easily incorporated to the system to enable the deposition of
232 materials not available at room temperature.

233 Capability to deposit dense thin layers over porous tubular supports enables the use of SALD for the
234 coating of dense membranes as well as other electrochemical devices such as fuel cells/electrolyzers or
235 electrochemical membrane reactors with tailored electrodes ⁴²⁻⁵¹, where the gas separation occurs by
236 adsorption and diffusion through the thin layer. Different ionic and protonic materials comprising more
237 complex oxides or metals have already been deposited by ALD ⁵²⁻⁶⁰, and their addition to the SALD
238 palette for both planar and tubular depositions would be appealing for various industrial applications.
239 Moreover, the gas manifold design could be adapted for the coating of other types of non-planar
240 substrates, which could be used in various applications such as free-form electronics ⁶¹ or for curved
241 lenses and mirrors fabrication ^{62,63}.

242 SALD gas manifolds can be also modular (coupling several manifolds in series) enlarging the
243 deposition area. This can be also used to tailor deposition i.e. different modules with alternating materials
244 can be used to have multimaterial and multifunctional devices.

245 4. Conclusions

246 In this work, we successfully performed thin film deposition on tubular substrates using the
247 atmospheric pressure SALD technique in the open-air close-proximity approach. Using computational
248 fluid dynamics calculations, an innovative SALD gas manifold has been designed and fabricated thanks
249 to the versatility offered by 3D printing. The custom gas manifold has been designed to deliver a
250 concentric homogeneous precursor gas outflow covering the whole surface of tubular substrates. The

251 relations between the different volumes within the gas manifolds has been evaluated by means of COMSOL
252 Multiphysics. Using DEZ and water as precursors, the design of the gas manifold has been validated by
253 depositing ZnO onto Cu foils and porous alumina tubular supports. The successful depositions show the
254 high potential of SALD for the engineering of membrane interfaces. Further optimization will result in
255 heads in which the ALD and CVD mode can be precisely controlled by adjusting the different flows.
256 These results open the door to the high-throughput fabrication of both dense and porous tubular
257 membranes of various materials by SALD. This approach can be further adapted to the preparation of
258 other nanomaterials as well as to other substrate geometries, widening the field of applications of SALD
259 on complex surfaces.

260 AUTHOR INFORMATION

261 **Corresponding Author**

262 * Corresponding author 1. *E-mail address:* fitolrei@itq.upv.es (D. Fidel Toldrá Reig)

263 ** Corresponding author 2. *E-mail address:* david.munoz-rojas@grenoble-inp.fr (D. Muñoz-Rojas)

264 **Present Addresses**

265 † Current Address: Instituto de Tecnología Química (CSIC-UPV), Universitat Politècnica de València,
266 Camino de vera s/n, 46022, Valencia, Spain

267 **Author Contributions**

268 The manuscript was written through contributions of all authors. All authors have given approval to the
269 final version of the manuscript.

270 **Funding Sources**

271 This work was supported by the French Research National Agency through the project ALD4MEM (ANR
272 ANR-20-CE09-0008).

273 **Acknowledgments**

274 The authors thank the French Research National Agency for funding (ANR ANR-20-CE09-0008) and
275 Hervé Roussel from LMGP for the XRD characterizations.

- 277 (1) Zydney, A. L. *Membrane Handbook*, Winston Ho, W. S.; Sirkar, K.K.; Reinhold, V.N.; Eds.; John
278 Wiley & Sons, Ltd, New York, 1992, AIChE J. 41 **1995**, 2343–2344.. DOI:
279 10.1002/AIC.690411024.
- 280 (2) *Comprehensive Membrane Science and Engineering (Second Edition)* Drioli, E.; Giorno, L.,
281 Fontananova, E., Eds. ; Elsevier: London, **2017**.
- 282 (3) Ivanova, M. E.; Escolástico, S.; Balaguer, M.; Palisaitis, J.; Sohn, Y. J.; Meulenber, W. A.;
283 Guillon, O.; Mayer, J.; Serra, J. M. Hydrogen Separation through Tailored Dual Phase Membranes
284 with Nominal Composition BaCe_{0.8}Eu_{0.2}O_{3-δ}:Ce_{0.8}Y_{0.2}O_{2-δ} at Intermediate Temperatures.
285 *Nat. Publ. Gr.* **2016**, 6, 34773. DOI: 10.1038/srep34773.
- 286 (4) Iwahara, H.; Asakura, Y.; Katahira, K.; Tanaka, M. Prospect of Hydrogen Technology Using
287 Proton-Conducting Ceramics. In *Solid State Ionics* **2004**, 168, 299–310. DOI:
288 10.1016/j.ssi.2003.03.001.
- 289 (5) Gallucci, F.; Medrano, J. A.; Fernandez, E.; Melendez, J.; Van Sint Annaland, M.; Pacheco-
290 Tanaka, D. A. Advances on High Temperature Pd-Based Membranes and Membrane Reactors for
291 Hydrogen Purification and Production. *Journal of Membrane Science and Research.* **2017**, 3, 142–
292 156. DOI: 10.22079/jmsr.2017.23644.
- 293 (6) Jeong, S. W.; Yamaguchi, T.; Okamoto, M.; Zhu, C.; Habazaki, H.; Nagayama, M.; Aoki, Y.
294 Proton Pumping Boosts Energy Conversion in Hydrogen-Permeable Metal-Supported Protonic
295 Fuel Cells. *ACS Appl. Energy Mater.* **2020**, 3 (1), 1222–1234. DOI: 10.1021/acsaem.9b02287.
- 296 (7) Meng, T.; Young, K.; Beglau, D.; Yan, S.; Zeng, P.; Cheng, M. M.-C. Hydrogenated Amorphous
297 Silicon Thin Film Anode for Proton Conducting Batteries. *J. Power Sources* **2016**, 302, 31–38.
298 DOI: 10.1016/J.JPOWSOUR.2015.10.045.
- 299 (8) Itoh, N.; Xu, W. .; Hara, S.; Sakaki, K. Electrochemical Coupling of Benzene Hydrogenation and
300 Water Electrolysis. *Catal. Today* **2000**, 56 (1–3), 307–314. DOI: 10.1016/S0920-5861(99)00288-
301 6.
- 302 (9) Serra, J. M. Electrifying Chemistry with Protonic Cells. *Nat. Energy* **2019**, 4 (3), 178–179. DOI:
303 10.1038/s41560-019-0353-y.
- 304 (10) Escorihuela, S.; Toldra-Reig, F.; Escolástico, S.; Murciano, R.; Martínez, A.; Serra, J. M. Copper
305 Surface-Alloying of H₂-Permeable Pd-Based Membrane for Integration in Fischer–Tropsch
306 Synthesis Reactors. *J. Memb. Sci.* **2021**, 619, 118516. DOI: 10.1016/j.memsci.2020.118516.
- 307 (11) Solís, C.; Toldra-Reig, F.; Balaguer, M.; Somacescu, S.; Garcia-Fayos, J.; Palafox, E.; Serra, J. M.
308 Mixed Ionic–Electronic Conduction in NiFe₂O₄–Ce_{0.8}Gd_{0.2}O_{2-δ} Nanocomposite Thin Films
309 for Oxygen Separation. *ChemSusChem* **2018**, 11, 2818–2827. DOI: 10.1002/cssc.201800420.
- 310 (12) Malerød-Fjeld, H.; Clark, D.; Yuste-Tirados, I.; Zanón, R.; Catalán-Martinez, D.; Beeff, D.;
311 Morejudo, S. H.; Vestre, P. K.; Norby, T.; Haugsrud, R.; Serra, J. M.; Kjølseth, C. Thermo-
312 Electrochemical Production of Compressed Hydrogen from Methane with near-Zero Energy Loss.
313 *Nat. Energy* **2017**, 2 (12), 923–931. DOI: 10.1038/s41560-017-0029-4.
- 314 (13) Arratibel Plazaola, A.; Pacheco Tanaka, D. A.; Van Sint Annaland, M.; Gallucci, F. Recent
315 Advances in Pd-Based Membranes for Membrane Reactors. *Molecules* **2017**, 22, 51 DOI:
316 10.3390/molecules22010051.
- 317 (14) Merlo, A.; Léonard, G. Magnetron Sputtering vs. Electrodeposition for Hard Chrome Coatings: A

- 318 Comparison of Environmental and Economic Performances **2021**, *14* (14), 3823. DOI:
319 10.3390/MA14143823/S1.
- 320 (15) Weber, M.; Julbe, A.; Kim, S. S.; Bechelany, M. Atomic Layer Deposition (ALD) on Inorganic or
321 Polymeric Membranes. *J. Appl. Phys.* **2019**, *126* (4), 041101. DOI: 10.1063/1.5103212.
- 322 (16) Weber, M.; Julbe, A.; Ayrál, A.; Miele, P.; Bechelany, M. Atomic Layer Deposition for
323 Membranes: Basics, Challenges, and Opportunities. *Chem. Mater.* **2018**, *30* (21), 7368–7390. DOI:
324 10.1021/acs.chemmater.8b02687.
- 325 (17) Yang, H. C.; Waldman, R. Z.; Chen, Z.; Darling, S. B. Atomic Layer Deposition for Membrane
326 Interface Engineering. *Nanoscale*. Royal Society of Chemistry November 28, 2018, pp 20505–
327 20513. DOI: 10.1039/c8nr08114j.
- 328 (18) George, S. M. Atomic Layer Deposition: An Overview. *Chem. Rev.* **2010**, *110* (1), 111–131. DOI:
329 10.1021/cr900056b.
- 330 (19) Johnson, R. W.; Hultqvist, A.; Bent, S. F. A Brief Review of Atomic Layer Deposition: From
331 Fundamentals to Applications. *Mater. Today* **2014**, *17* (5), 236–246. DOI:
332 10.1016/j.mattod.2014.04.026.
- 333 (20) Leskelä, M.; Ritala, M. Atomic Layer Deposition (ALD): From Precursors to Thin Film Structures.
334 *Thin Solid Films* **2002**, *409* (1), 138–146. DOI: 10.1016/S0040-6090(02)00117-7.
- 335 (21) Muñoz-Rojas, D.; Macmanus-Driscoll, J. Spatial Atmospheric Atomic Layer Deposition: A New
336 Laboratory and Industrial Tool for Low-Cost Photovoltaics. *Materials Horizons* **2014**, *1*, 314–320.
337 DOI: 10.1039/c3mh00136a.
- 338 (22) Muñoz-Rojas, D.; Maindrón, T.; Esteve, A.; Píallat, F.; Kools, J. C. S.; Decams, J.-M. Speeding
339 up the Unique Assets of Atomic Layer Deposition. *Mater. Today Chem.* **2019**, *12*, 96–120. DOI:
340 10.1016/J.MTCHEM.2018.11.013.
- 341 (23) Musselman, K. P.; Muñoz-Rojas, D.; Hoye, R. L. Z.; Sun, H.; Sahonta, S. L.; Croft, E.; Böhm, M.
342 L.; Ducati, C.; MacManus-Driscoll, J. L. Rapid Open-Air Deposition of Uniform, Nanoscale,
343 Functional Coatings on Nanorod Arrays. *Nanoscale Horizons* **2017**, *2* (2), 110–117. DOI:
344 10.1039/C6NH00197A.
- 345 (24) Nguyen, V. S.; Sekkat, A.; Bellet, D.; Chichignoud, G.; Kaminski-Cachopo, A.; Muñoz-Rojas, D.;
346 Favre, W. Open-Air, Low-Temperature Deposition of Phase Pure Cu₂O Thin Films as Efficient
347 Hole-Transporting Layers for Silicon Heterojunction Solar Cells. *J. Mater. Chem. A* **2021**, *9* (29),
348 15968–15974. DOI: 10.1039/D1TA02931B.
- 349 (25) Nguyen, V. H.; Resende, J.; Papanastasiou, D. T.; Fontanals, N.; Jiménez, C.; Muñoz-Rojas, D.;
350 Bellet, D. Low-Cost Fabrication of Flexible Transparent Electrodes Based on Al Doped ZnO and
351 Silver Nanowire Nanocomposites: Impact of the Network Density †. *Nanoscale* **2019**, *11*, 12097.
352 DOI: 10.1039/c9nr02664a.
- 353 (26) Muñoz-Rojas, D.; Huong Nguyen, V.; Masse de la Huerta, C.; Jiménez, C.; Bellet, D. Spatial
354 Atomic Layer Deposition. In *Chemical Vapor Deposition for Nanotechnology*; IntechOpen, **2019**.
355 DOI: 10.5772/intechopen.82439.
- 356 (27) Levy, D. H.; Freeman, D.; Nelson, S. F.; Cowdery-Corvan, P. J.; Irving, L. M. Stable ZnO Thin
357 Film Transistors by Fast Open Air Atomic Layer Deposition. *Appl. Phys. Lett.* **2008**, *92* (19). DOI:
358 10.1063/1.2924768.
- 359 (28) Muñoz-Rojas, D.; Sun, H.; Iza, D. C.; Weickert, J.; Chen, L.; Wang, H.; Schmidt-Mende, L.;
360 MacManus-Driscoll, J. L. High-Speed Atmospheric Atomic Layer Deposition of Ultra Thin

- 361 Amorphous TiO₂ Blocking Layers at 100 °C for Inverted Bulk Heterojunction Solar Cells. *Prog.*
362 *Photovoltaics Res. Appl.* **2013**, 21 (4), 393–400. DOI: 10.1002/PIP.2380.
- 363 (29) Levy David H. Process for Atomic Layer Deposition. US-7413982-B2, **2008**.
- 364 (30) de la Huerta, C. A. M.; Nguyen, V. H.; Sekkat, A.; Crivello, C.; Toldra-Reig, F.; Veiga, P. B.;
365 Quessada, S.; Jimenez, C.; Muñoz-Rojas, D. Gas-Phase 3D Printing of Functional Materials. *Adv.*
366 *Mater. Technol.* **2020**, 5, 2000657. DOI: 10.1002/admt.202000657.
- 367 (31) Muñoz-Rojas, D.; Weber, M.; Va L L É E, C.; Crivello, C.; Sekkat, A.; Toldra-Reig, F.; Bechelany,
368 M. Nanometric 3D Printing of Functional Materials by Atomic Layer Deposition. *Adv. Addit.*
369 *Manuf.; IntechOpen*, **2022**. DOI: 10.5772/INTECHOPEN.101859.
- 370 (32) Ommen, J. R. van; Kooijman, D.; Niet, M. de; Talebi, M.; Goulas, A. Continuous Production of
371 Nanostructured Particles Using Spatial Atomic Layer Deposition. *J. Vac. Sci. Technol. A Vacuum,*
372 *Surfaces, Film.* **2015**, 33 (2), 021513. DOI: 10.1116/1.4905725.
- 373 (33) Li, J.; Pumera, M. 3D Printing of Functional Microrobots. *Chem. Soc. Rev.* **2021**, 50 (4), 2794–
374 2838. DOI: 10.1039/D0CS01062F.
- 375 (34) Browne, M. P.; Plutnar, J.; Pourrahimi, A. M.; Sofer, Z.; Pumera, M. Atomic Layer Deposition as
376 a General Method Turns Any 3D-Printed Electrode into a Desired Catalyst: Case Study in
377 Photoelectrochemistry. *Adv. Energy Mater.* **2019**, 9 (26), 1900994.
- 378 (35) Ng, S.; Zazpe, R.; Rodriguez-Pereira, J.; Michalička, J.; Macak, J. M.; Pumera, M. Atomic Layer
379 Deposition of Photoelectrocatalytic Material on 3D-Printed Nanocarbon Structures. *J. Mater.*
380 *Chem. A* **2021**, 9 (18), 11405–11414.
- 381 (36) Nguyen, V. H.; Resende, J.; Jiménez, C.; Deschanvres, J.-L.; Carroy, P.; Muñoz, D.; Bellet, D.;
382 Muñoz-Rojas, D. Deposition of ZnO Based Thin Films by Atmospheric Pressure Spatial Atomic
383 Layer Deposition for Application in Solar Cells. *J. Renew. Sustain. Energy* **2017**, 9 (2), 021203.
384 DOI: 10.1063/1.4979822.
- 385 (37) Nguyen, V. H.; Sekkat, A.; Masse De La Huerta, C. A.; Zoubian, F.; Crivello, C.; Rubio-Zuazo, J.;
386 Rubio-Zuazo, J.; Jaffal, M.; Bonvalot, M.; Vallée, C.; Aubry, O.; Rabat, H.; Hong, D.; Muñoz-
387 Rojas, D. Atmospheric Plasma-Enhanced Spatial Chemical Vapor Deposition of SiO₂ Using
388 Trivinylmethoxysilane and Oxygen Plasma. *Chem. Mater.* **2020**, 32 (12), 5153–5161. DOI:
389 10.1021/ACS.CHEMMATER.0C01148.
- 390 (38) de la Huerta, C. M.; Nguyen, V. H.; Dedulle, J. M.; Bellet, D.; Jiménez, C.; Muñoz-Rojas, D.
391 Influence of the Geometric Parameters on the Deposition Mode in Spatial Atomic Layer
392 Deposition: A Novel Approach to Area-Selective Deposition. *Coatings* **2018**, 9 (1), 5. DOI:
393 10.3390/COATINGS9010005.
- 394 (39) Nguyen, V. H.; Sekkat, A.; Jiménez, C.; Muñoz, D.; Bellet, D.; Muñoz-Rojas, D. Impact of
395 Precursor Exposure on Process Efficiency and Film Properties in Spatial Atomic Layer Deposition.
396 *Chem. Eng. J.* **2021**, 403, 126234. DOI: 10.1016/j.cej.2020.126234.
- 397 (40) Weber, M.; Drobek, M.; Rebière, B.; Charmette, C.; Cartier, J.; Julbe, A.; Bechelany, M. Hydrogen
398 Selective Palladium-Alumina Composite Membranes Prepared by Atomic Layer Deposition. *J.*
399 *Memb. Sci.* **2020**, 596, 117701. DOI: 10.1016/j.memsci.2019.117701.
- 400 (41) Weber, M.; Bechelany, M. Combining Nanoparticles Grown by ALD and MOFs for Gas
401 Separation and Catalysis Applications. *Pure Appl. Chem.* **2020**, 92 (2), 213–222. DOI:
402 10.1515/PAC-2019-0109.
- 403 (42) Vøllestad, E.; Strandbakke, R.; Tarach, M.; Catalán-Martínez, D.; Fontaine, M. L.; Beeff, D.;

- 404 Clark, D. R.; Serra, J. M.; Norby, T. Mixed Proton and Electron Conducting Double Perovskite
405 Anodes for Stable and Efficient Tubular Proton Ceramic Electrolysers. *Nat. Mater.* **2019**, *18* (7),
406 752–759. DOI: 10.1038/s41563-019-0388-2.
- 407 (43) Morejudo, S. H.; Zanón, R.; Escolástico, S.; Yuste-Tirados, I.; Malerød-Fjeld, H.; Vestre, P. K.;
408 Coors, W. G.; Martínez, A.; Norby, T.; Serra, J. M.; Kjølseth, C. Direct Conversion of Methane to
409 Aromatics in a Catalytic Co-Ionic Membrane Reactor. *Science* (80-.). **2016**, *353* (6299), 563–566.
410 DOI: 10.1126/SCIENCE.AAG0274.
- 411 (44) Tan, X. Y.; Yin, W. N.; Meng, B.; Meng, X. X.; Yang, N. T.; Ma, Z. F. Preparation of Electrolyte
412 Membranes for Micro Tubular Solid Oxide Fuel Cells. *Sci. China Ser. B Chem.* **2008**, *51*
413 (9), 808–812. DOI: 10.1007/S11426-008-0068-6.
- 414 (45) Zhu, L.; O’Hayre, R.; Sullivan, N. P. High Performance Tubular Protonic Ceramic Fuel Cells via
415 Highly-Scalable Extrusion Process. *Int. J. Hydrogen Energy* **2021**, *46* (54), 27784–27792. DOI:
416 10.1016/J.IJHYDENE.2021.06.018.
- 417 (46) Agbede, O. O.; Hellgardt, K.; Kelsall, G. H. Electrical Conductivities and Microstructures of LSM,
418 LSM-YSZ and LSM-YSZ/LSM Cathodes Fabricated on YSZ Electrolyte Hollow Fibres by Dip-
419 Coating. *Mater. Today Chem.* **2020**, *16*, 100252. DOI: 10.1016/J.MTCHEM.2020.100252.
- 420 (47) Kleiminger, L.; Li, T.; Li, K.; Kelsall, G. H. Syngas (CO-H₂) Production Using High Temperature
421 Micro-Tubular Solid Oxide Electrolysers. *Electrochim. Acta* **2015**, *179*, 565–577. DOI:
422 10.1016/J.ELECTACTA.2015.07.062.
- 423 (48) Morales, M.; Laguna-Bercero, M. A. Microtubular Solid Oxide Fuel Cells Fabricated by Gel-
424 Casting: The Role of Supporting Microstructure on the Mechanical Properties. *RSC Adv.* **2017**, *7*
425 (29), 17620–17628. DOI: 10.1039/C7RA01259D.
- 426 (49) Kherad, R.; Dodangei, S.; Moussavi, S. H.; Ghatee, M. Characterization of Anode Supported
427 Micro-Tubular Solid Oxide Fuel Cells Prepared by Successive Non-Aqueous Electrophoretic
428 Deposition. *J. Electroceramics* **2021**, *1*, 1–7. DOI: 10.1007/S10832-021-00272-5.
- 429 (50) Li, Y.; Chen, L.; Zhang, L.; Xia, C. Millimeter Tubular Solid Oxide Electrolysis Cells with
430 Modified Asymmetric Hydrogen Electrode. *Int. J. Hydrogen Energy* **2016**, *41* (10), 5209–5214.
431 DOI: 10.1016/J.IJHYDENE.2016.01.103.
- 432 (51) Tan, Z.; Ishihara, T. Effect of Ni-Based Cathodic Layer on Intermediate Temperature Tubular
433 Electrolysis Cell Using LaGaO₃-Based Electrolyte Thin Film. *JPhys Energy* **2020**, *2* (2), 024004.
434 DOI: 10.1088/2515-7655/ab6f4b.
- 435 (52) Gong, T.; Huang, Y.; Qin, L.; Zhang, W.; Li, J.; Hui, L.; Feng, H. Atomic Layer Deposited
436 Palladium Nanoparticle Catalysts Supported on Titanium Dioxide Modified MCM-41 for Selective
437 Hydrogenation of Acetylene. *Appl. Surf. Sci.* **2019**, *495*, 143495. DOI:
438 10.1016/J.APSUSC.2019.07.237.
- 439 (53) Chen, R.; Qu, K.; Li, J.; Zhu, P.; Duan, C.; Zhang, J.; Li, X.; Liu, X.; Yang, Z. Ultrathin Zirconia
440 Passivation and Stabilization of Aluminum Nanoparticles for Energetic Nanomaterials via Atomic
441 Layer Deposition. *ACS Appl. Nano Mater.* **2018**, *1* (10), 5500–5506. DOI:
442 10.1021/acsanm.8b01005.
- 443 (54) Park, J.; Lee, Y.; Chang, I.; Cho, G. Y.; Ji, S.; Lee, W.; Cha, S. W. Atomic Layer Deposition of
444 Yttria-Stabilized Zirconia Thin Films for Enhanced Reactivity and Stability of Solid Oxide Fuel
445 Cells. *Energy* **2016**, *116*, 170–176. DOI: 0.1016/J.ENERGY.2016.09.094.
- 446 (55) Oh, S.; Park, J.; Shin, J. W.; Yang, B. C.; Zhang, J.; Jang, D. Y.; An, J. High Performance Low-

- 447 Temperature Solid Oxide Fuel Cells with Atomic Layer Deposited-Yttria Stabilized Zirconia
448 Embedded Thin Film Electrolyte. *J. Mater. Chem. A* **2018**, *6* (17), 7401–7408. DOI:
449 10.1039/C7TA10678E.
- 450 (56) Fan, L.; Zhu, B.; Su, P. C.; He, C. Nanomaterials and Technologies for Low Temperature Solid
451 Oxide Fuel Cells: Recent Advances, Challenges and Opportunities. *Nano Energy* **2018**, *45*, 148–
452 176. DOI: 10.1016/j.nanoen.2017.12.044.
- 453 (57) Pessoa, R. S.; Fraga, M. A.; Chiappim, W.; Maciel, H. S. Exploring the Properties and Fuel Cell
454 Applications of Ultrathin Atomic Layer Deposited Metal Oxide Films. *Emerg. Mater. Energy*
455 *Convers. Storage*, Cheong, K.Y.; Impellizzeri, G.; Fraga, M.A.; Eds.; El Sevier, London, **2018**,
456 83–114. DOI: 10.1016/B978-0-12-813794-9.00003-X.
- 457 (58) Shim, J. H.; Chao, C. C.; Huango, H.; Prinz, F. B. Atomic Layer Deposition of Yttria-Stabilized
458 Zirconia for Solid Oxide Fuel Cells. *Chem. Mater.* **2007**, *19* (15), 3850–3854. DOI:
459 10.1021/cm070913t.
- 460 (59) Shim, J. H.; Park, J. S.; An, J.; Gür, T. M.; Kang, S.; Prinz, F. B. Intermediate-Temperature Ceramic
461 Fuel Cells with Thin Film Yttrium-Doped Barium Zirconate Electrolytes. *Chem. Mater.* **2009**, *21*
462 (14), 3290–3296. DOI: 10.1021/cm900820p.
- 463 (60) Park, J. S.; Kim, Y. B.; Shim, J. H.; Kang, S.; Gür, T. M.; Prinz, F. B. Evidence of Proton Transport
464 in Atomic Layer Deposited Yttria-Stabilized Zirconia Films. *Chem. Mater.* **2010**, *22* (18), 5366–
465 5370. DOI: 10.1021/cm1017536.
- 466 (61) Konda, A.; Rau, A.; Stoller, M. A.; Taylor, J. M.; Salam, A.; Pribil, G. A.; Argyropoulos, C.; Morin,
467 S. A. Soft Microreactors for the Deposition of Conductive Metallic Traces on Planar, Embossed,
468 and Curved Surfaces. *Adv. Funct. Mater.* **2018**, *28* (40). DOI: 10.1002/ADFM.201803020.
- 469 (62) Tian, M.; Su, Y.; Zheng, H.; Pei, G.; Li, G.; Riffat, S. A Review on the Recent Research Progress
470 in the Compound Parabolic Concentrator (CPC) for Solar Energy Applications. *Renew. Sustain.*
471 *Energy Rev.* **2018**, *82*, 1272–1296. DOI: 10.1016/J.RSER.2017.09.050.
- 472 (63) Ko, H. C.; Stoykovich, M. P.; Song, J.; Malyarchuk, V.; Choi, W. M.; Yu, C. J.; Geddes, J. B.;
473 Xiao, J.; Wang, S.; Huang, Y.; Rogers, J. A. A Hemispherical Electronic Eye Camera Based on
474 Compressible Silicon Optoelectronics. *Nat.* **2008**, *454* (7205), 748–753. DOI:
475 10.1038/nature07113.

476

477

478

479

480

481

482

483

484

485

486

487

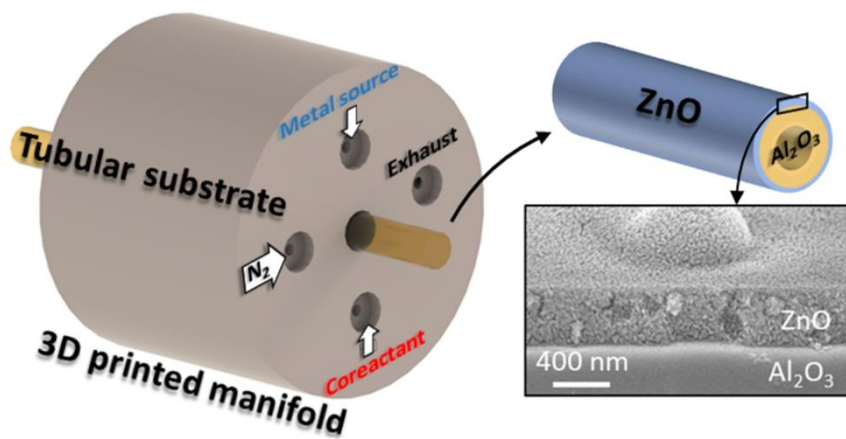
488

489

490

491

For Table of Contents Use Only



492

493 3D-printed spatial atomic layer deposition gas manifold for coating of non-planar substrates like tubular
494 samples

495